coatings

MDPI

Article

Fatigue and Life Prediction of S135 High-Strength Drill Pipe Steel under Tension–Torsion Multiaxial Loading

Sheji Luo [1], Ming Liu [2,*], Lihong Han [3,*] and Yuna Xue [1]

[1] School of Materials Science and Engineering, Xi'an Shiyou University, Xi'an 710065, China; sjluo@xsyu.edu.cn (S.L.); xynlina@163.com (Y.X.)
[2] Center for Advancing Materials Performance from the Nanoscale (CAMP-Nano), State Key Laboratory for Mechanical Behavior of Materials, Xi'an Jiaotong University, Xi'an 710049, China
[3] State Key Laboratory of Service Behavior and Structure Safety for Petroleum Tubular Goods and Equipment Material, CNPC Tubular Goods Research Institute, Xi'an 710077, China
* Correspondence: liuming0313@xjtu.edu.cn (M.L.); hanlihong@cnpc.com.cn (L.H.)

Abstract: This paper investigates the fatigue behavior of S135 high-strength drill pipe steel under tension–torsion multiaxial loading. Based on the concept of critical plane during fatigue, the fatigue model under the combined loading of tension–torsion is established. The proposed model is validated, and the predicted results are in good agreement with the experimental testing results. The maximum relative errors between the estimation and the experiment are mostly within the range of factor two to three for proportional, and 90° non-proportional tension–torsion loading. Meanwhile, the failure mechanism is also discussed through fracture analysis.

Keywords: fatigue; high-strength steel; prediction; multiaxial; tension–torsion

Citation: Luo, S.; Liu, M.; Han, L.; Xue, Y. Fatigue and Life Prediction of S135 High-Strength Drill Pipe Steel under Tension–Torsion Multiaxial Loading. *Coatings* **2022**, *12*, 1222. https://doi.org/10.3390/coatings12081222

Academic Editors: Filippo Berto and Giorgos Skordaris

Received: 26 July 2022
Accepted: 19 August 2022
Published: 21 August 2022

1. Introduction

Most of the components in engineering are subjected to multiaxial loads. Even if the component itself works under a uniaxial load, notches or corrosion defects of the complex lead to a multiaxial stress state in local area, which leads to fatigue failure [1–6]. Therefore, the study of multiaxial fatigue is much closer to the engineering practice than that of uniaxial fatigue, and how to prevent multiaxial fatigue failure becomes extremely important in engineering practice [7,8]. Multiaxial fatigue refers to the fatigue under the action of multiple stresses or strains. Multiaxial fatigue damage occurs under multiaxial cyclic loading, during which two or three components of stress (or strain) change independently with time. The changes of these stress (strain) components may be in phase and proportional, or out of phase and non-proportional [9–11].

As an important structure in petroleum, natural gas and geological exploration, the drill pipe is mainly subjected to tension, compression, bending, twisting, and vibration loads, and also bears internal and external pressure, rotating centrifugal force, and other additional loadings [12–15]. The working conditions of a drill pipe are severe, and fatigue failure is inevitable. In addition, due to the bending of the well bore, "dogleg" or horizontal drilling, the drill pipe is bent through the "dogleg" during rotation (see Figure 1), and is not only subjected to tension–compression loading but also torque, thus, resulting in severe fatigue damage [16–18]. Failure analysis shows that the macroscopic fracture of the drill pipe presents a stepped shape, and then propagation deviates from the vertical direction of the drill pipe axis. Path I is an proportional loading path, where the axial and torsional loads are increased and decreased proportionally during a loading cycle. Path III is a circular-shaped, non-proportional loading path typically used in the study of multiaxial fatigue. Path III is often referred to as the 90°out-of-phase loading.

Hence, for most cases, the fatigue failure of the drill pipe is considered to be caused by the I–III combined axial torsional loading [19,20].

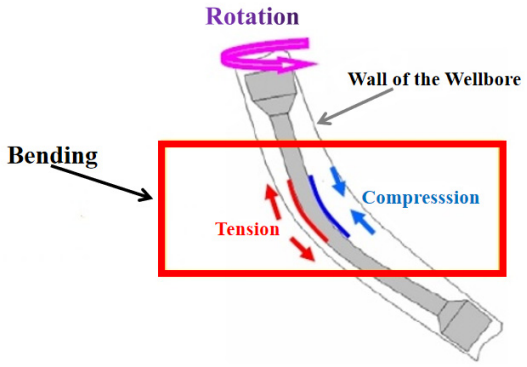

Figure 1. Schematic illustration of dogleg.

In our previous work, we studied the uniaxial fatigue behaviors of S135 drill pipe steel in various conditions [21–23]. The results show that the fatigue limit of torsional fatigue compared to that of tension–compression fatigue is reduced by 31.84%. Meanwhile, the fracture analysis shows torsional fatigue produces more fatigue damage at the same stress level. In this paper, the fatigue lives of S135 steel were tested under proportional and 90° non-proportional tension–torsion multiaxial loadings. The expression of fatigue life was obtained, the fracture mechanism was analyzed, and the prediction model was established. The model proposed in this paper could be used to predict the fatigue life of drill pipe steel. Also, the results could provide theoretical support for the study of multiaxial fatigue, and technical support for the selection of drill pipe steels.

2. Experimental Section

2.1. Materials

The experimental material was S135 high-strength drill pipe steel. The chemical compositions (in % by mass) determined by analytical analysis are 0.20 C, 0.24 Si, 0.54 Mn, 0.007 P, 0.0035 S, 0.403 Ni, 0.861 Cr, 0.858 Mo, 0.007 Ti, 0.06 Cu, and any remaining percentage is Fe. The fatigue specimens were along the vertical of drill pipe, and then were machined into round rods with a diameter Φ = 5 mm base on the Chinese standard GB/T 3075, as shown in Figure 2. All specimens were polished from grit 200 to 2000 step by step with SiC sandpaper prior to the experiment.

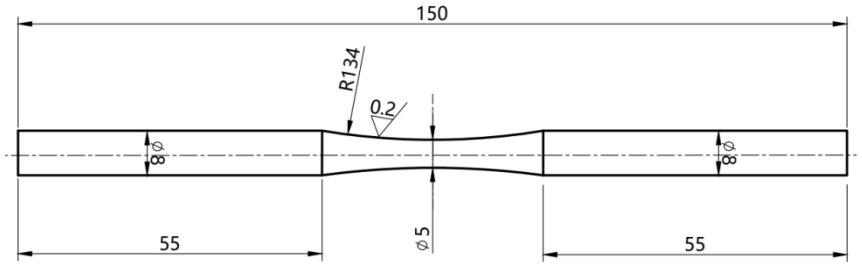

Figure 2. Schematic illustration of fatigue specimen (all units in mm).

The tensile test was performed on a WDS-100 electronic universal testing machine (Guan Jing Electric Instrument Equipment Co., Ltd., Beijing, China) with a loading rate of 0.2 mm/min and a strain rate of 10^{-3}/s corresponding to sample spacing.

2.2. Fatigue Test

The tension–torsion fatigue tests were carried out on a PLD-50KN-250NM electro-hydraulic servo fatigue test machine (Lichuang Material Testing Technology Co., Ltd., Xi'an, China), which can control both axial and radial direction so multiaxial fatigue loading can be achieved. Symmetrical loading was adopted, i.e., the loading tension stress ratio $R_\sigma = \sigma_{min}/\sigma_{max}$ was −1, the loading shear stress ratio $R_\tau = \tau_{min}/\tau_{max}$ was −1, the τ_a/σ_{eq} was 0.7, the loading was in-phase proportional, and the phase angle was 0° and 90°, respectively. Figure 3 shows the proportional loading path and 90°out-of-phase loading path. During the actual drilling process, the speed of a drill pipe is usually between 120~180 r/min (2~3 Hz), so the loading frequency was 3 Hz, and triangular waves were adopted. Three tests were performed at each stress level. The fracture surfaces of the specimens were observed by JSM-6390A scanning electron microscope (SEM, kabuskiki kaisha, Tokyo, Japan), and the accelerating voltage was 20 kV. All the experiments were carried out in the air.

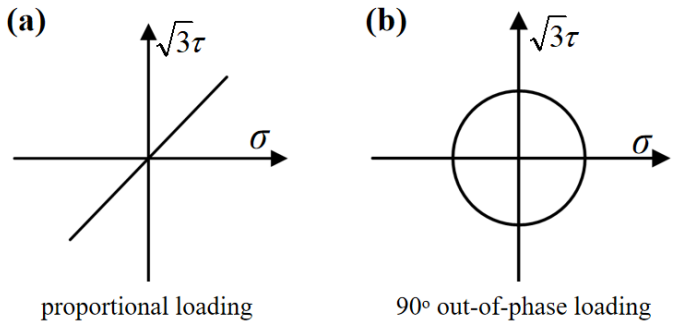

Figure 3. The load path of tension–torsion corrosion fatigue (stress control). (**a**) proportional loading and (**b**) 90o out-of-phase loading

3. Results and Discussion

3.1. Stress–Strain Curve

The tested stress–strain curve of S135 steel is shown in Figure 4. It can be seen that the steel is a continuously strain-hardening material, with an obvious physical yielding phenomenon, and the stress–strain curve becomes flat after yielding. The yield strength and tensile strength are 935 and 1058 MPa, respectively.

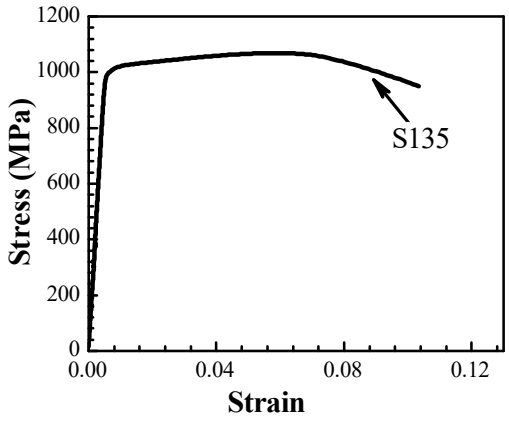

Figure 4. Stress–strain curve of S135 steel.

3.2. Proportional Tension–Torsion Loading

3.2.1. Fatigue Life and S-N Curve

Table 1 shows the fatigue life of S135 drill pipe steel under the proportional tension–torsion loading. Fatigue limit refers to the stress of material without fracture after infinite cycles. Generally, it is considered that the stress value corresponds to 10^7 cycles without fracture for carbon steel. In Table 1, when the equivalent stress is 509.6 MPa, the maximum number of cycles is 5.90×10^6, which is close to 10^7 cycles, indicating that the stress is close to the tensile–torsion fatigue limit of the material.

Table 1. Fatigue test results of proportional tension–torsion loading.

No.	P_{max}/kN	S_{eq} /MPa	M_{max} /N·m	τ_a /MPa	N_f /cycles
1	15	763.0	13.125	535.03	4785
2	15	763.0	13.125	535.03	5673
3	15	763.0	13.125	535.03	8974
4	14	713.3	12.25	499.4	8705
5	14	713.3	12.25	499.4	17,250
6	14	713.3	12.25	499.4	10,456
7	12	611.5	10.5	428.0	83,155
8	12	611.5	10.5	428.0	49,646
9	12	611.5	10.5	428.0	31,087
10	11	560.5	9.625	392.3	163,603
11	11	560.5	9.625	392.3	109,413
12	11	560.5	9.625	392.3	201,298
13	10.5	535.0	9.1875	375.0	261,066
14	10.5	535.0	9.1875	375.0	180,658
15	10.5	535.0	9.1875	375.0	461,559
16	10	509.6	8.75	356.7	2.65×10^6, fracture
17	10	509.6	8.75	356.7	5.21×10^6, fracture
18	10	509.6	8.75	356.7	5.90×10^6, fracture

Figure 5 shows the relationship between the fatigue life of S135 steel and the amplitude of tensile and compressive stress under proportional tension–torsion loading. The fatigue life exceeds 10^5 cycles when the tensile and compressive stress amplitude decrease to about 550 MPa. With the decrease in the tensile and compressive stress amplitude level, the fatigue life is significantly prolonged, showing obvious characteristics of fatigue limit. Based on our previous study [15], the strength corresponding to the 10 million cycles of S135 steel is about 510 MPa. Since the stress state of the tension–torsion loading is more complex than that of the uniaxial loading, its fatigue limit is completely reduced. The fatigue life in this study is very close to 10^7 when the S_{eq} is 509.6 Mpa, so the experiment under lower stress was not carried out. The fatigue life is close to 10^7 cycles, and tends to be infinite when the amplitude of the tensile and compressive stress is reduced below 500 MPa.

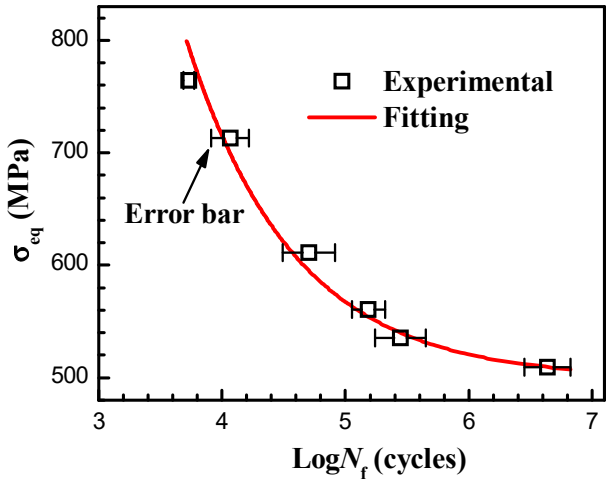

Figure 5. Testing results and fitting curve of tension–torsion fatigue lives under proportional loading.

Based on the equation of symmetrical cyclic stress fatigue life in the whole life range [24], the effective stress S_a is the main factor that controls the fatigue life in the tension–torsion loading. Thus, the equivalent stress S_{eq} and the fatigue limit $(S_{eq})_c$ can be reasonably used to replace the S_a and S_c, respectively. The fatigue life equation under tension–torsion loading can be obtained as follow [24,25]:

$$N_f = A^*[S_{eq} - (S_{eq})_c]^{-2} \quad (1)$$

where A^* is the fatigue resistance coefficient and $(S_{eq})_c$ is the theoretical fatigue limit. The fatigue life is finite when $S_{eq} > (S_{eq})_c$, the fatigue life tends to be infinite when $S_{eq} \le (S_{eq})_c$.

The equivalent stress amplitude can be obtained [12]:

$$S_{eq} = \sqrt{\frac{1}{2(1-R)}}\Delta\sigma = \sqrt{\frac{1}{2(1-R)}}\sigma_{max}(1-R) \quad (2)$$

where $\Delta\sigma$, σ_{max} , and R are the stress range, maximum stress, and stress ratio, respectively. During the fatigue test, the yield strength of 0.65 times was chosen for the test, and it is found that fatigue life is in the 10^4 cycles range; in order to obtain the data from 10^3 or so, stress higher than the initial value 100 MPa was used. Then, the initial down load was 50 MPa below the 0.65 times yield strength. The load was constantly adjusted during the experiment, in order to obtain a complete fatigue life curve.

Taking the logarithm on both sides of Equation (1):

$$\lg N_f = \lg A^* - 2\lg[S_{eq} - (S_{eq})_c] \quad (3)$$

Equation (3) represents a straight line with a slope of -2 in the double logarithmic coordinate of $\lg N_f$ - $\lg[S_{eq}$ - $(S_{eq})_c]$, and then the fatigue life of S135 steel under proportional loading can be obtained by regression analysis using the tail difference method:

$$N_f = 4.40\times10^8(S_{eq} - 499.0)^{-2} \quad (4)$$

The fitting curve is in good agreement with the experimental results, as shown in Figure 5. The linear correlation coefficient $|r|$ is 0.9773, which is greater than the minimum value of 0.798, corresponding to 99% confidence. Therefore, Equation (1) can be well-used to describe the general rule of fatigue life of S135 steel under proportional tension–torsion loading. Thus, Equation (4) can be used to predict the fatigue damage of

components, as long as the external force is determined. In addition, the above equation can also be applied to Al and its alloys [24–26], although the specific parameters may be different. We have added those examples from the literature to the references section.

3.2.2. Fatigue Fracture Mechanisms

Figure 6 shows the macroscopic morphologies of the fatigue fracture specimen under proportional tension–torsion loading with different stress amplitudes. The fatigue initiation zone appears gray–black due to the repeated tension–compression and torsion loading. The proportion of each area changes with the different stress amplitudes. Under the loading of tension–torsion, the specimen shows a brittle fracture with no obvious plastic deformation, because the fracture is uneven. Under the shear stress of the torque, the cross-section and the axial direction of the specimen are approximately 45°, the fatigue crack is formed from the surface and propagates to the interior of the specimen, and multiple fatigue initiations are observed. Then, the so-called "roof ridge" feature is formed by the connection of different fatigue initiations and the action of composite loading.

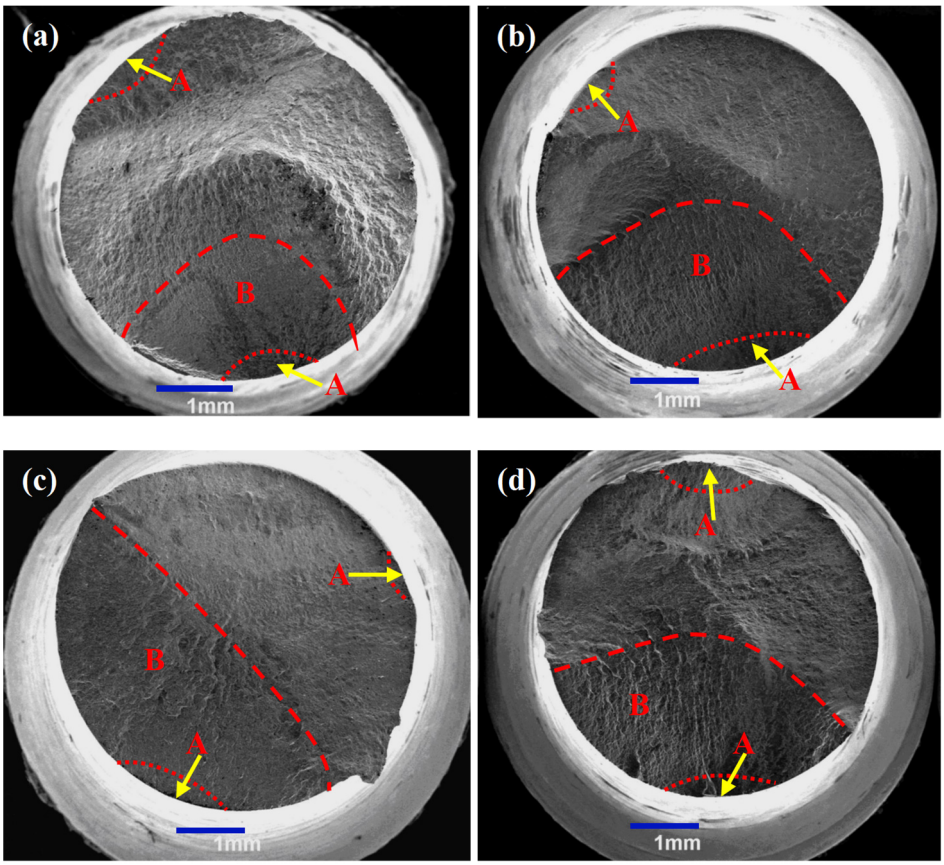

Figure 6. Macroscopic morphologies of fatigue fracture under proportional tension–torsion loading at different stress amplitudes. (**a**) S_{eq} = 509.6 MPa, (**b**) S_{eq} = 560.5 MPa, (**c**) S_{eq} = 611.5 MPa, (**d**) S_{eq} = 713.3 MPa. 'A' represents fatigue initiation zone and 'B' represents fatigue crack propagation zone.

Figure 7 shows the morphologies of the crack source zone of the steel under the proportional tension–torsion loading with different stress amplitudes. It can be seen that the fatigue crack initiates on, or near the surface of, the steel. Due to the repeat opening and closing, the fracture surface in the fatigue initiation zone is smoother. The cracks start from the initiation point and propagate forward in a fluvial pattern, then deviate from the propagation direction due to different resistance. After that, the cracks begin to expand on their own planes to form steps, which form radial rays on the fracture surface. With the increase in stress amplitudes, the river pattern decreases, and scratch marks are

detected. No obvious fatigue striations are observed in this zone, and the larger the stress amplitudes, the smaller the area of this zone.

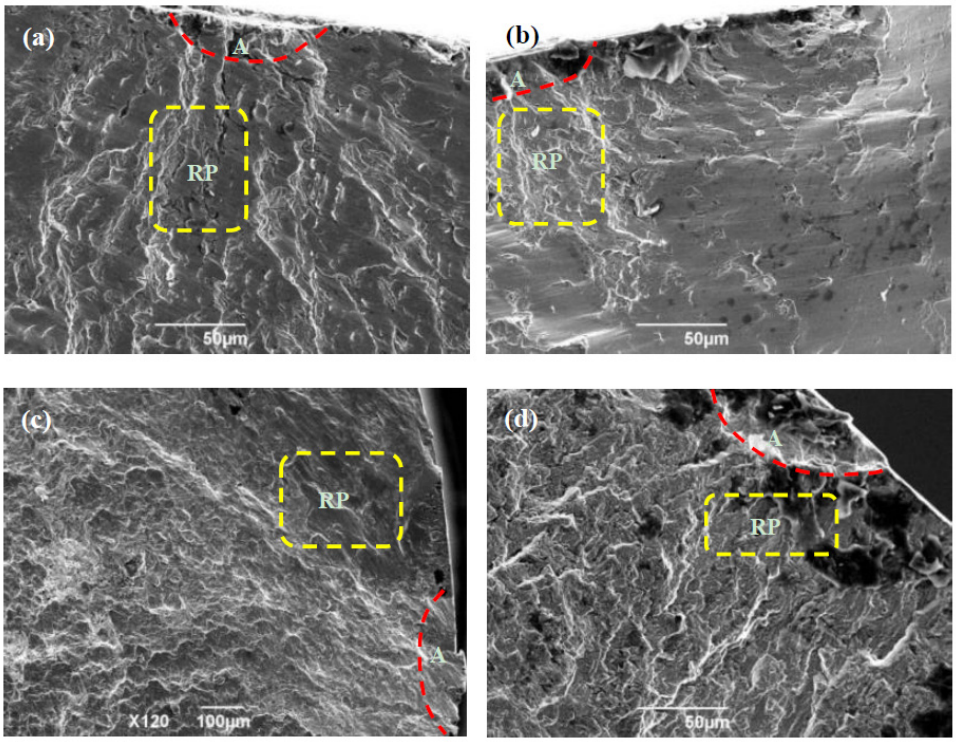

Figure 7. Fracture morphologies of fatigue crack initiation region under proportional tension–torsion loading at different stress amplitudes. (**a**) S_{eq} = 560.5 MPa, (**b**) S_{eq} = 611.5 MPa, (**c**) S_{eq} = 713.3 MPa, (**d**) S_{eq} = 763 MPa. 'A' represents fatigue initiation zone and 'RP' represents river pattern.

Figure 8 shows the morphologies of the crack propagation zone of the fatigue fracture specimen under the proportional tension–torsion loading with different stress amplitudes. It can be seen that a transgranular fracture is the main feature. The fatigue striations are perpendicular to the crack propagation direction, and the secondary cracks are at a certain angle to the main crack when the tensile stress amplitude S_{eq} is 560.5 MPa. The fracture surface is composed of some parallel stripes, which are mainly perpendicular to the crack propagation direction and are not as sharp as the fatigue striations, showing an obvious ripple pattern. No obvious fatigue striations are observed on the fracture surface when the tensile stress amplitude S_{eq} is 611.5 MPa. The size of the ripple pattern area is related to the stress amplitude level. With the increase in the half stress amplitude, the ripple pattern area increases.

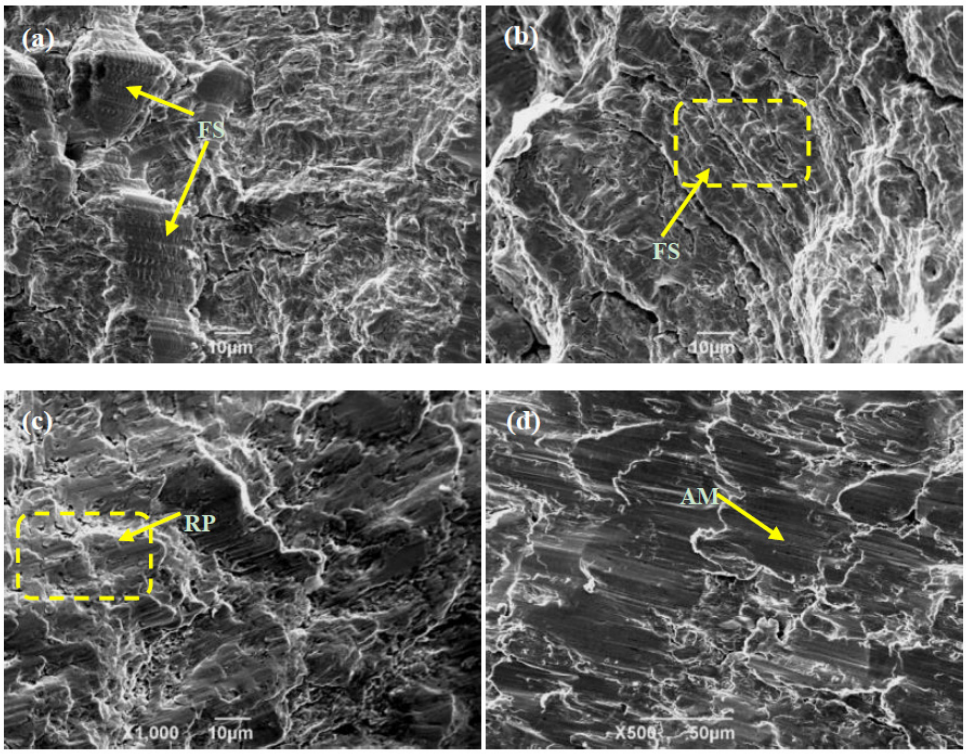

Figure 8. Fracture morphologies of fatigue crack propagation zone under proportional tension–torsion loading at different stress amplitudes. (**a**) S_{eq} = 560.5 MPa, (**b**) S_{eq} = 611.5 MPa, (**c**) S_{eq} = 713.3 MPa, (**d**) S_{eq} = 763 MPa. 'FS' represents fatigue striations, 'RP' represents river pattern, and 'AM' represents abrasion marks.

3.3. Non-Proportional Tension–Torsion Loading

3.3.1. Fatigue Life and S–N Curve

Table 2 shows the fatigue life of S135 steel under 90° non-proportional tension–torsion loading. It can be seen that with the decrease in stress amplitude, the tension–torsion fatigue life of the material is prolonged. The fatigue life of the sample reaches 2.65 × 10^6 cycles when the tensile and compressive stress amplitude is reduced to 458.6 MPa, indicating that the stress is close to the tension–torsion fatigue limit of the material.

Table 2. Fatigue test results under 90° non-proportional tension–torsion loading.

No.	P_{max}/kN	S_{eq}/MPa	M_{max}/N·m	τ_a/MPa	N_f/Cycles
1	14	713.3	12.25	499.4	5230
2	14	713.3	12.25	499.4	3972
3	14	713.3	12.25	499.4	2685
4	13	662.4	11.375	467.3	4138
5	13	662.4	11.375	467.3	16,230
6	13	662.4	11.375	467.3	7835
7	11	560.5	9.625	392.3	36,720
8	11	560.5	9.625	392.3	26,478
9	11	560.5	9.625	392.3	52,467
10	10	509.6	8.75	356.7	143,852
11	10	509.6	8.75	356.7	199,838
12	10	509.6	8.75	356.7	394,570
13	9.5	486	8.3125	338.9	1.58×10^6

14	9.5	486	8.3125	338.9	524,780
15	9.5	486	8.3125	338.9	981,740
16	9	458.6	7.875	321.0	1.52×10^6, fracture
17	9	458.6	7.875	321.0	6.23×10^6, fracture
18	9	458.6	7.875	321.0	6.48×10^6, fracture

Figure 9 shows the relationship between the fatigue life of 90° non-proportional tension–torsion loading and the amplitude of tension–compression when the τ_a / S_{eq} is 0.7. When the tensile and compressive stress amplitude decreases to about 500 MPa, the fatigue life exceeds 10^5 cycles. When the amplitude of the tensile and compressive stress decreases below 450 Mpa, the fatigue life is close to 10^7 cycles, and tends to have infinite life.

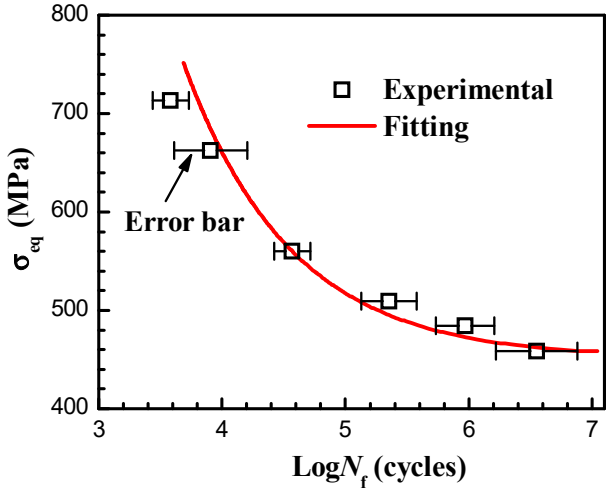

Figure 9. Testing results and fitting curve of tension–torsion fatigue lives under 90° non-proportional loading.

The fatigue life of S135 steel under 90° non-proportional loading can be fitted by Equation (1):

$$N_f = 4.36 \times 10^8 (S_{eq} - 449.2)^{-2} \quad (5)$$

It can be seen from Figure 9 that the fitting curve is in good agreement with the experimental results. The linear correlation coefficient |r| is 0.9474, which is greater than the minimum value of 0.605, corresponding to 99% confidence. Therefore, Equation (1) can be well-used to describe the general rule of fatigue life of S135 steel under 90° non-proportional tension–torsion loading.

Under non-proportional loading, the strain principal axis rotates in the cyclic process because of the phase difference of the applied tension–torsion strain components [27]. This rotation means both the shear strain and the normal strain on the maximum shear plane cannot reach the maximum at the same time. Moreover, because of the phase difference between the two, they interact with each other to produce an additional hardening phenomenon [28,29]. The 90° non-proportional circular paths have the greatest additional enhancement.

3.3.2. Fatigue Fracture Mechanisms

The macro morphologies of 90° non-proportional tension–torsion loading fatigue fracture specimens under different stress amplitudes are displayed in Figure 10. It can be seen that fatigue crack presents as multiple sources that originate from the surface of the maximum equivalent stress. After the fatigue crack initiation, the crack propagates into

the interior of the material until it is unstable. The crack propagation section is at a certain angle to the loading direction, and the fracture surface of the horizontal specimen is perpendicular to the loading direction under lower normal stress. The fractured specimen has no obvious plastic deformation, and typical fatigue fracture characteristics are observed. With the increase in tensile stress amplitude, the proportion of the crack source zone decreases. An obvious crack source zone can be seen on the fracture surface when the stress amplitude S_{eq} is 458.6 MPa. However, when the tensile stress amplitude S_{eq} increases to 662.4 MPa, no distinct macroscopic crack source zone can be seen, and the proportion of the instantaneous fracture zone increases.

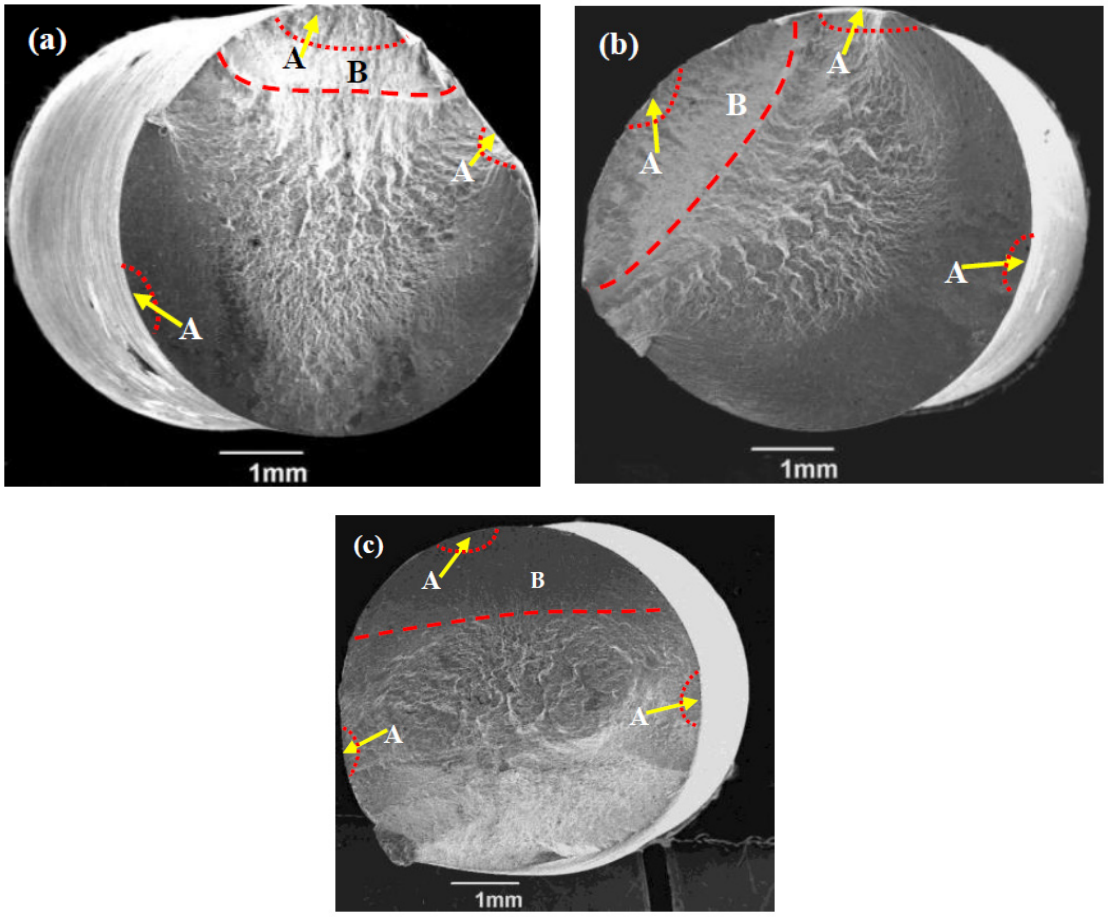

Figure 10. Macroscopic fatigue fracture morphologies of different stress amplitudes under 90° non-proportional tension–torsion loading. (**a**) S_{eq} = 458.6 MPa, (**b**) S_{eq} = 509.6 MPa, (**c**) S_{eq} = 622.4 MPa. 'A' represents fatigue initiation zone and 'B' represents fatigue crack propagation zone.

The microfracture morphologies of the 90° non-proportional tension–torsion fatigue crack source zone under different stress amplitudes are shown in Figure 11. It can be seen that the crack source zone is mainly characterized as a cleavage fracture. With the increase in stress amplitude, the proportion of cleavage surface increases and scratch marks are observed. The fracture is dominated by tearing edge and cleavage plane when σ_{eq} is 458.6 MPa; there are a few river patterns and a lot of scratch marks when σ_{eq} is 662.4 MPa. The fatigue cracks originate on, or near the surface of, the material, and the area of the fatigue initiation zone is also the smallest. After crack initiation, it propagates outward in the form of radiation. Later, with the increase in crack propagation rate, the convergence degree of radiation decreases. The crack source formation point is about 500 μm × 450 μm and 200

μm × 170 μm when the σ_{eq} is 458.6 and 509.6 MPa respectively. When the σ_{eq} is 622.4 MPa, the area of crack source area is much smaller. Lots of scratch marks are observed because of the repeated axial and torsional stresses.

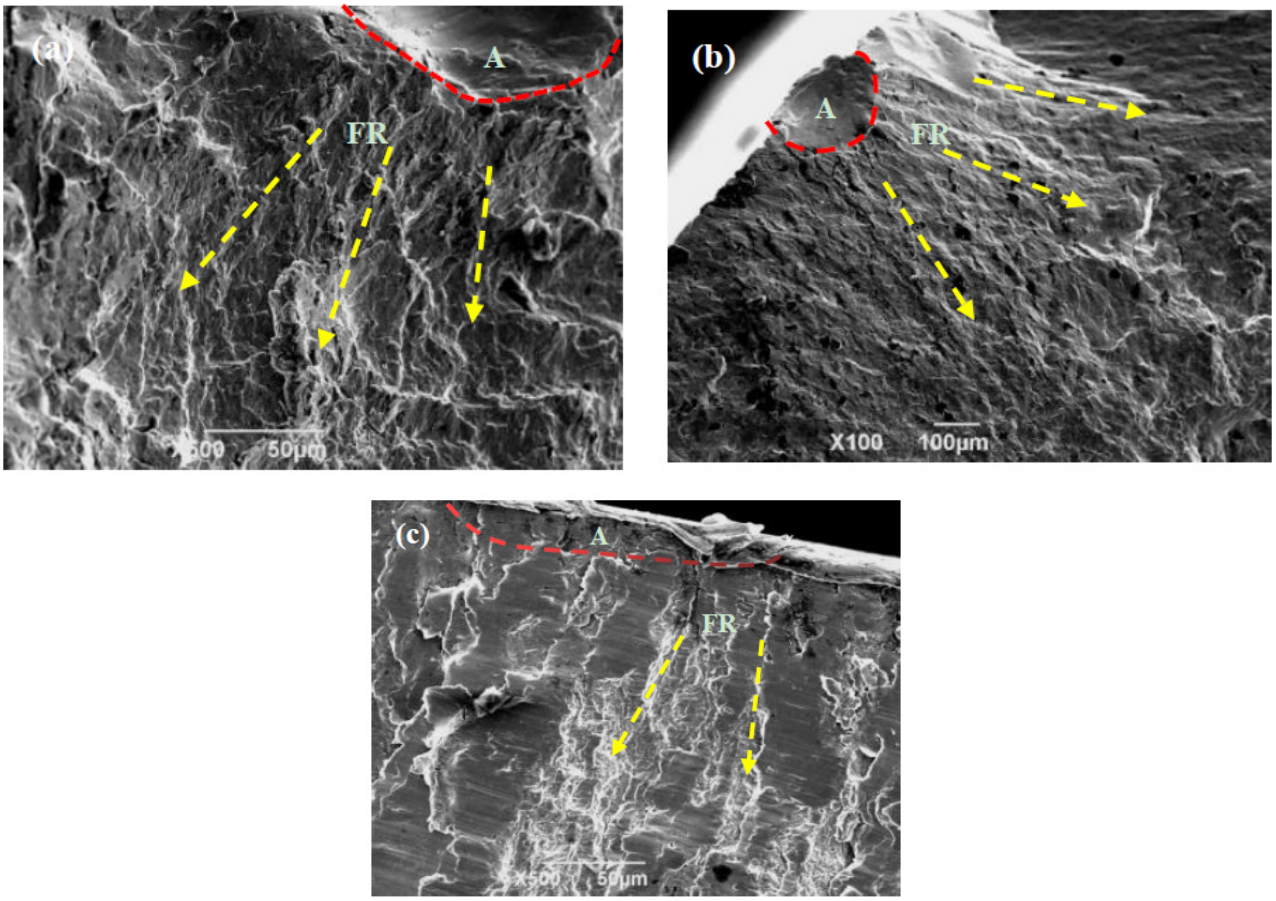

Figure 11. Fracture morphologies of fatigue crack initiation region under 90° non-proportional tension–torsion loading at different stress amplitudes. (**a**) S_{eq} = 458.6 MPa, (**b**) S_{eq} = 509.6 MPa, (**c**) S_{eq} = 622.4 MPa. 'A' represents fatigue initiation zone and 'FR' represents fatigue radiation.

Figure 12 shows the microfracture morphologies of the crack propagation zone under 90° non-proportional tension–torsion loading under different stress amplitudes. The fatigue crack propagation zone is mainly characterized as the tearing edges formed by the connection between different fracture surfaces, a relatively flat cleavage plane is formed between the tearing edges. Regular fine steps are formed in the direction perpendicular to the tearing edge, which is caused by cyclic shear stresses. A small number of steps, similar to the fatigue striations, are observed in the fatigue crack propagation zone when the loading is lower. There are small steps between the tearing edges that are regularly and densely arranged around the tearing edges when the loading S_{eq} is 458.6 MPa; with the increase in the loading stress amplitude S_{eq}, the spacing between the fine steps and the tearing edges increases, and a small number of secondary cracks are observed (see Figure 12b); large-scale transgranular cracks are seen when the loading stress S_{eq} is 622.4 MPa (see Figure 10c).

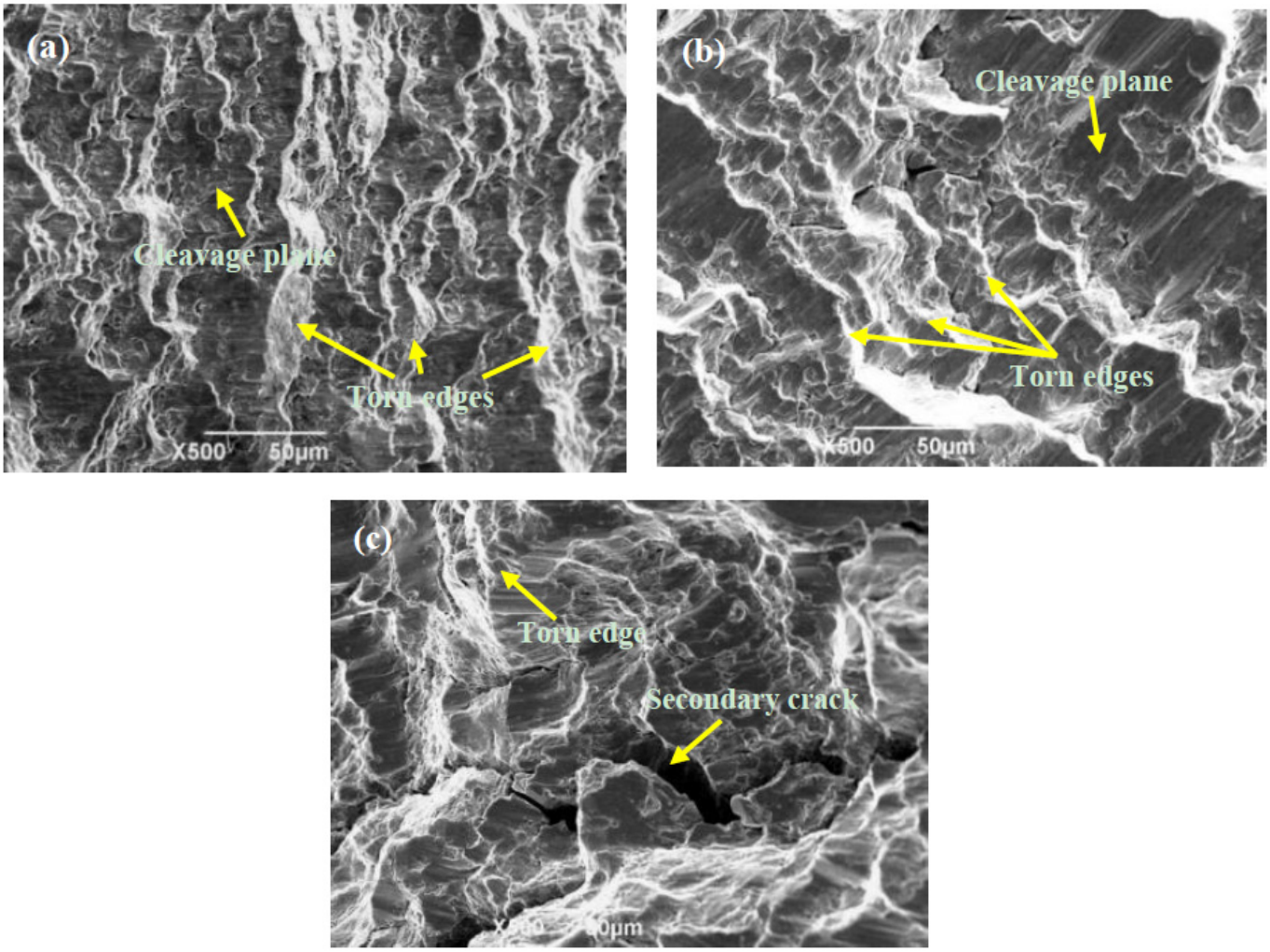

Figure 12. Fracture morphologies of fatigue crack propagation zone under 90° non-proportional tension–torsion loading at different stress amplitudes. (**a**) S_{eq} = 458.6 MPa, (**b**) S_{eq} = 509.6 MPa, (**c**) S_{eq} = 622.4 MPa.

3.4. Fatigue Quantitative Model

3.4.1. Basic Assumptions

There have been plenty of attempts in the field of multiaxial fatigue modeling [30,31], and here, we also propose a model to predict the multiaxial fatigue behavior of drill pipe steel. Since the crack in the persistent slip band is the result of the sliding of the micro-zone along the metal slip surface under the action of external forces, the slip of the micro-zone depends on the orientation of the grain and the loading mode. During tension–compression fatigue loading, the direction of the maximum shear stress to the loading axis is 45° [32]. After cracking in the slip zone, the crack expands in stage I to form the initial macroscopic crack, and then enters stage II to expand. However, under the torsion loads, the direction of the maximum shear stress and the resident slip is perpendicular to the axis of the specimen and longitudinal. After cracking in the slip zone, the crack expands within stage I to form the initial macroscopic crack, and then enters stage II to expand. The crack propagation in both sections is perpendicular to the axis of the sample. Therefore, it can be reasonably assumed that the fatigue crack is formed in the persistent slip band on the surface of the sample, and then cracks along the slip surface of the grain.

The fatigue crack propagation in stage I with crystallographic characteristics accounts for most of the fatigue life.

3.4.2. Fatigue Critical Plane

The critical plane method considers that the fatigue failure occurs in a specific plane, where the accumulation of fatigue damage and the estimation of fatigue life are carried out. This method is based on the fracture model and crack initiation mechanism. Figure 13 summarizes the critical surfaces of tension–compression, torsion, and tension–torsion fatigues. Theoretically, the angle θ between the critical surface of tension–compression and torsion fatigue is 45°, so the critical surface of tension–torsion fatigue should be located between them, which is the direction of the maximum shear stress.

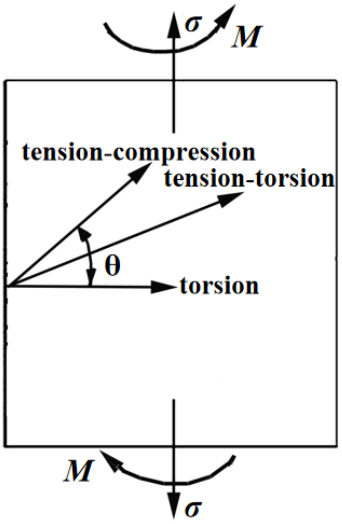

Figure 13. Critical plane of fatigue formation.

From the microscopic point of view, the fatigue limit can be considered as the point of whether the dislocation on the critical plane or the slip plane produces alternating slip. The slip of dislocation on the critical plane is caused by shear stress, the critical shear stress for dislocation alternating slip should be the same regardless of the critical plane, and the critical shear stress should be equal to the fatigue limit expressed by shear stress. Therefore, the fatigue limit obtained under different loading modes is equivalent. The θ in Figure 13 under proportional loading is $\pi/4$. The normal stress under tension–compression loading is equivalent to the maximum stress; thus, the fatigue life can be obtained by substituting $S_{\mathrm{eqv}} = \tau_a \cos\pi/4$ in $N_f = 4.64\times10^8 (S_{\mathrm{eqv}} - 577.9)^{-2}$:

$$\mathrm{N_f} = 3.28\times10^8 (\tau_\mathrm{a} - 408.6)^{-2} \quad (6)$$

Comparing Equation (6) to the torsion fatigue experiment results $N_f = 1.66\times10^8 (\tau_a - 393.9)^{-2}$ [33], the maximum relative error of the fatigue limit is only 3.73%, and the maximum relative error of the fatigue resistance coefficient is 39.8%. Therefore, the S135 steel belongs to the sliding surface cracking, and the equations of symmetric tension fatigue life are equivalent to that of torsion.

Under multiaxial fatigue, the bearing of the critical plane is related to the direction of the average principal stress, which refers to the angle between the average direction of the maximum principal stress and the critical plane. It can be estimated by the following empirical equation [34]:

$$\delta = \frac{3\pi}{8}\left[1 - \left(\frac{t_{af,-1}}{S_{af,-1}}\right)^2\right] \quad (7)$$

where $t_{af,-1}$ and $S_{af,-1}$ are the torsional and tension–compression fatigue strength for a given number of cycles, respectively. For extremely hard, brittle materials, $t_{af,-1} = S_{af,-1}$, $\delta = 0$; for materials with good toughness, $\sqrt{3}t_{af,-1} = S_{af,-1}$, $\delta = 45$. For medium carbon S135 steel, the orientation of the average critical surface $\delta = 36.14^{\circ}$, which can be obtained by substituting torsion and tensile fatigue strength into Equation (7).

3.4.3. Proportional Fatigue Life Equation

Under tensile–torsional fatigue loading, the fatigue crack forms on the critical surface, which is the slip surface of the crystal, while the fatigue crack forms along the slip surface. The fatigue cracking of S135 steel has crystallographic characteristics, and conforms to the basic characteristics of the fracture in the fatigue initiation zone.

Findley and Matake proposed the linear combination of shear stress amplitude and normal stress amplitude on the critical surface as the stress criterion for multiaxial fatigue [35,36]:

$$\tau_{ns,a} + kS_{n,a} = q \tag{8}$$

where $\tau_{ns,a}$ and $S_{n,a}$ are the allowable alternating stress and maximum normal stress, respectively; k and q are the material constants, k is relatively small for ductile materials and larger for brittle material, and q can be determined by shear cracking [37]:

$$q = \tau_c \left(\frac{N_\tau}{N_f}\right)^{1/m_\tau} \tag{9}$$

where N_τ and N_f are the cycles corresponding to the symmetric torsion fatigue limit τ_c and the fatigue cycles of the *S–N* curve respectively, and m_τ is the exponent ($\tau_a = CN_f^{1/m_\tau}$) of the symmetric torsion fatigue *S–N* curve. Therefore, q specifies the fatigue strength of cycle times N_f under multiaxial loading, and $\tau_{ns,a} + kS_{n,a}$ is the effective shear stress amplitude of the critical surface under multiaxial fatigue.

Substituting $\tau_{ns,a} + kS_{n,a}$ into the torsion fatigue life equation $N_f = A'(\tau_a - \tau_c)^{-2}$, then the fatigue life equation under tension–torsion loading can be obtained:

$$N_f = A'(\tau_a + kS_a - \tau_c)^{-2} \tag{10}$$

The value of k can be determined by the experimental results. τ_a is the fatigue limit under tension–torsion loading ($\tau_a / S_a = 0.7$) when $N_f \to \infty$, the fatigue limit expressed in shear stress amplitude $\tau_{t-t,c}$ (the fatigue limit in of $N_f = 3.09\times10^8(\tau_a - 347.8)^{-2}$) can be obtained:

$$k = (\tau_c - \tau_{t-t,c}) / S_{t-t,c} = (393.9 - 347.8)/499 = 0.092 \tag{11}$$

Substituting A', k, and τ_C into Equation (10), the specific expression of tension–torsion fatigue life of S135 steel can be obtained:

$$N_f = 1.66\times10^8(\tau_a + 0.092S_a - 393.9)^{-2} \tag{12}$$

Then the specific criterion for fatigue failure of S135 steel under tension–torsion loading can be obtained:

$$\tau_a + 0.092S_a = 393.9 + 1.29\times10^4 / N_f^{0.5} \tag{13}$$

3.4.4. Non-Proportional Fatigue Life Equation

For non-proportional loading, non-proportional factors are usually induced to reflect the influence of the loading path on fatigue life [38]:

$$D_{np} = D(1+\alpha\varphi) \tag{14}$$

where D_{np} and D are the fatigue damage parameters of non-proportional loading and proportional loading, respectively; α is the material sensitive constants of non-proportional loading; φ is the non-proportional factors, which can be determined by the ratio of the short axis to the long axis of the strain channel ellipse, when τ_a / S_a is 0.7, φ equals 0.404.

Taking D_{np} as the shear stress amplitude, the fatigue life under non-proportional loading can be obtained by substituting Equation (14) into Equation (10):

$$N_f = A'[(\tau_a + kS_a)(1+\alpha\varphi) - \tau_c)^{-2} \tag{15}$$

The value of α can be determined by the experiment testing. Under tension–torsion fatigue (τ_a / S_a = 0.7), τ_a is the fatigue limit under non-proportional loading when $N_f \to \infty$, then the fatigue limit $\tau_{t-t,np,c}$ expressed in shear stress amplitude ($N_f = 3.05\times10^8(\tau_a - 314.7)^{-2}$) can be obtained:

$$\begin{aligned}\alpha = [\tau_c /(\tau_{t-t,np,c} + kS_{t-t.np,c}) - 1]/\varphi &= \text{-}[1-393.9/(317 + 0.092\times449.2)]/0.404 \\ &= 0.263\end{aligned} \tag{16}$$

Substituting A' , k , τ_C , α , and φ into Equation (15), the specific expression of fatigue life of S135 steel under 90° non-proportional tension–torsion loading can be obtained:

$$N_f = 1.66\times10^8[1.106\times(\tau_a + 0.092S_a) - 393.9]^{-2} \tag{17}$$

Hence, the specific fatigue failure criterion of S135 steel under 90° non-proportional tension–torsion loading can be obtained:

$$\tau_a + 0.092S_a = [393.9 + 1.29\times10^4 / N_f{}^{0.5}]/1.106 \tag{18}$$

3.4.5. Contrastive Analysis

The fatigue life under the condition of τ_a / S_a = 0.7 is predicted by Equation (13), and the comparison with the experimental results is shown in Figure 14a. It is seen that the maximum relative errors between the estimation and the experiment are mostly within the range of two factors (with one exception); thus, Equation (13) can be well-used to estimate the fatigue life of S135 steel under the proportional tension–torsion loading.

Equation (18) is applied to predict the fatigue life under 90° non-proportional tension–torsion loading, and the predicted and the experimental results are shown in Figure 14b. It is seen that the errors between the predicted and the testing results are in the range of three factor for most the experimental tests. Therefore, Equation (18) can also be well-used to estimate the fatigue life of S135 steel under 90° non-proportional tension–torsion loading. Based on the predicted results in Figure 14, most of the predicted results are smaller than the experimental results, indicating that the predicted results of Equations (13) and (18) are conservative, which means the developed mode could be used in engineering practice. Our next work is to develop a general equation to describe multiaxial fatigue.

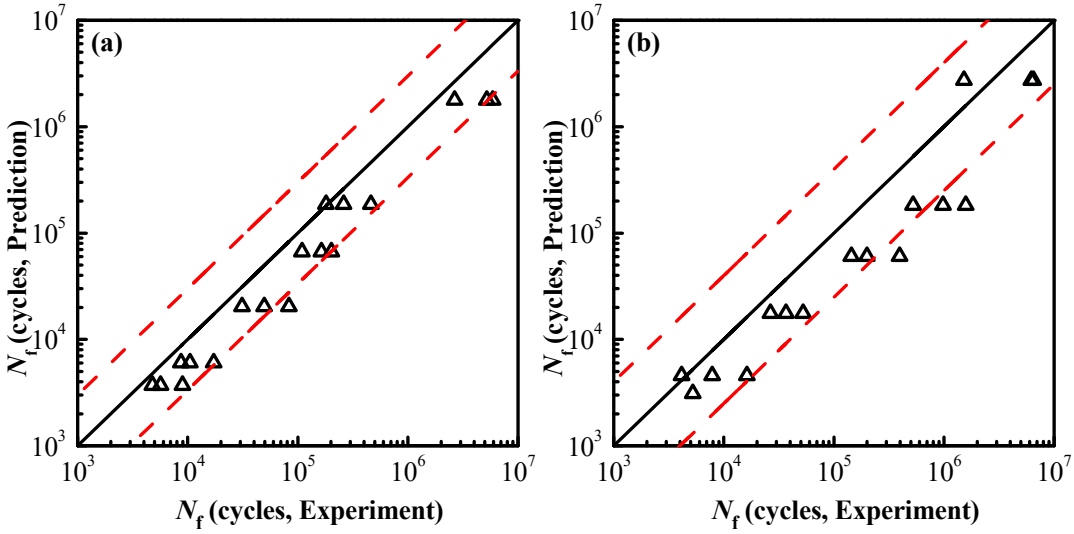

Figure 14. Predicted versus experimental live under proportional loading (**a**) and non-proportional loading (**b**).

4. Conclusions

The fatigue behavior of S135 high-strength drill pipe steel under the condition of tension–torsion loading was studied. Based on the fatigue critical plane, the fatigue model was established, and the fatigue fracture mechanism was analyzed. The main conclusions are as follows:

(1) The fatigue model of the S135 steel under the combined loading of tension–torsion is established: $N_f = A'[(\tau_a + kS_a)(1+\alpha\varphi) - \tau_c]^{-2}$, and the method to determine the weight k and the non-proportional sensitivity coefficient α is given. The specific expressions are $N_f = 1.66\times10^8(\tau_a + 0.092S_a - 393.9)^{-2}$ for proportional tension–torsion loading, and $N_f = 1.66\times10^8[1.106\times(\tau_a + 0.092S_a) - 393.9]^{-2}$ for non-proportional tension–torsion loading.;

(2) Under the proportional tension–torsion loading, the fatigue crack initiates on the surface of the specimen and propagates to the interior, which is often caused by multiple fatigue initiations that connect to form the so-called "ridge" feature; Under the condition of 90° non-proportional tension–torsion loading, the fatigue crack initiates at the maximum equivalent stress site of the specimen surface, and the fatigue crack often appears from multiple sources;

(3) The fracture source area of the proportional tension–torsion loading is characterized as an obvious fluvial pattern, and the crack propagation zone is characterized as fatigue striations and ripple patterns; the fracture source area of the 90° non-proportional tension–torsion loading is characterized as cleavage, the stable growth area is characterized as the tear edges formed by the connection between different fracture surfaces, and the tear edges are relatively flat.

Author Contributions: Conceptualization, S.L and M.L.; methodology, S.L.; validation, L.H.; formal analysis, M.L.; investigation, S.L.; resources, L.H.; data curation, M.L.; writing—original draft preparation, M.L.; writing—review and editing, M.L and S.L and Y.X.; visualization, M.L.; supervision, L.H.; project administration, L.H.; funding acquisition, L.H. All authors have read and agreed to the published version of the manuscript.

Funding: This research was funded by the Key Research and Development Plan of Shaanxi Province (No. 2017KJXX-03), the Shaanxi National Science Foundation (No. 2021JM-412, 2020JQ-773), the Innovation Team Funding by Xian Shiyou University (No. 2019QNKYCXTD12), and Xi'an Key Laboratory of High Performance Oil and Gas Field Materials, School of Material Science and Engineering, Xi'an Shiyou University.

Institutional Review Board Statement: Not applicable.

Informed Consent Statement: Not applicable.

Data Availability Statement: No data were used to support this study.

Conflicts of Interest: The authors declare no conflict of interest.

References

1. Far, A.H.; Anijdan, S.M.; Abbasi, S.M. The effect of increasing Cu and Ni on a significant enhancement of mechanical properties of high strength low alloy, low carbon steels of HSLA-100 type. *Mater. Sci. Eng. A* **2019**, *746*, 384–393.
2. Rahi, A. Lateral Vibration of a Micro Overhung Rotor-Disk Subjected to an Axial Load Based on the Modified Strain Gradient Theory. *Mech. Adv. Mater. Struct.* **2018**, *18*, 1850114.
3. Rajabinezhad, M.; Bahrami, A.; Mousavinia, M.; Seyedi, S.J.; Taheri, P. Corrosion-Fatigue Failure of Gas-Turbine Blades in an Oil and Gas Production Plant. *Materials* **2020**, *13*, 900.
4. Bisong, M.; Sivtsev, P.; Lepov, V. Numerical Analysis of Stress-Strain State and Crack Propagation in Welded Samples. *Solid State Phenom.* **2017**, *265*, 507–512.
5. Sabzi, M.; Dezfuli, S.M. Drastic improvement in mechanical properties and weldability of 316L stainless steel weld joints by using electromagnetic vibration during GTAW process. *J. Manuf. Processes* **2018**, *33*, 74–85.
6. Antsiferov, S.; Sammal, A.; Deev, P. Stress state estimation in multilayer support of vertical shafts, considering off-design cross-sectional deformation. *IOP Conf. Ser. Earth Environ. Sci.* **2018**, *134*, 012001.
7. Khorsov, P.; Laas, R.; Surzhikov, A.P. The Application of Reverberation in Method of Mechanoelectrical Transformations for Estimation of Stress-Strain State in Solid Dielectrical Matter. *Mater. Sci. Forum* **2019**, *970*, 47–54.
8. Tarasov, B.G.; Sadovskii, V.M.; Sadovskaya, O.V.; Cassidy, M.J.; Randolph, M.F. Modelling the static stress-strain state around the fan-structure in the shear rupture head. *Appl. Math. Model.* **2018**, *57*, 268–279.
9. Yan, Q.; Luo, M.; Tang, K. Multi-axis variable depth-of-cut machining of thin-walled workpieces based on the workpiece deflection constraint. *Comput. -Aided Des.* **2018**, *100*, 14–29.
10. Tian, Y.Z.; Sun, S.J.; Lin, H.R.; Zhang, Z.F. Fatigue behavior of CoCrFeMnNi high-entropy alloy under fully reversed cyclic deformation. *J. Mater. Sci. Technol.* **2018**, *35*, 334–340.
11. Mironov, V.I.; Ogorelkov, D.A.; Lukashuk, O.A. Analysis of Fatigue Damage Accumulation in Structural Materials under Quasi-Random Load. *Solid State Phenom.* **2020**, *299*, 1178–1183.
12. Luo, S.; Liu, M.; Shen, Y.; Lin, X. Sulfide Stress Corrosion Cracking Behavior of G105 and S135 High-Strength Drill Pipe Steels in H_2S Environment. *J. Mater. Eng. Perform.* **2019**, *28*, 1707–1718.
13. Zeng, D.; Li, H.; Tian, G.; Liu, F.; Li, B.; Yu, S.; Ouyang, Z.; Shi, T. Fatigue behavior of high-strength steel S135 under coupling multi-factor in complex environments. *Mater. Sci. Eng. A* **2018**, *724*, 385–402.
14. Zhao, T.; Liu, Z.; Du, C.; Dai, C.; Li, X.; Zhang, B. Corrosion fatigue crack initiation and initial propagation mechanism of E690 steel in simulated seawater. *Mater. Sci. Eng. A* **2017**, *708*, 181–192.
15. Han, L.; Liu, M.; Luo, S.; Lu, T.J. Fatigue and corrosion fatigue behavior of G105 and S135 high-strength drill pipe steels in air and H_2S environment. *Process Saf. Environ. Prot.* **2019**, *124*, 63–74.
16. Liu, W.; Liu, Y.; Chen, W.; Shi, T.; Singh, A.; Lu, Q. Longitudinal crack failure analysis of box of S135 tool joint in ultra-deep well. *Eng. Fail. Anal.* **2015**, *48*, 283–296.
17. Medjo, B.; Rakin, M.; Gubeljak, N.; Matvienko, Y.; Arsić, M.; Šarkoćević, Ž.; Sedmak, A. Failure resistance of drilling rig casing pipes with an axial crack. *Eng. Fail. Anal.* **2015**, *58*, 429–440.
18. May, M.E.; Saintier, N.; Palin-Luc, T.; Devos, O.; Brucelle, O. Modelling of corrosion fatigue crack initiation on martensitic stainless steel in high cycle fatigue regime. *Corros. Sci.* **2018**, *133*, 397–405.
19. Farhangdoost, K.; Siahpoosh, M. On The Fatigue Life Prediction of Die-Marked Drillpipes[C]. In Proceedings of the 2006 ASME Pressure Vessels and Piping Division Conference, Vancouver, BC, Canada, 23–27 July 2006; Volume 7, pp. 1–8.
20. Feng, M.; Ding, F.; Jiang, Y. A study of loading path influence on fatigue crack growth under combined loading. *Int. J. Fatigue* **2006**, *28*, 19–27.
21. Luo, S.; Liu, M.; Wen, N.; Shen, Y.; Liu, Y.M.; Lin, X.Z. Effect of pre-corrosion on electrochemical corrosion and fatigue behavior of S135 high-strength drill pipe steel in marine environment. *Int. J. Electrochem. Sci.* **2019**, *14*, 2589–2605.
22. Liu, M.; Luo, S.; Shen, Y. Corrosion fatigue crack propagation behaviour of S135 high-strength drill pipe steel in H_2S environment. *Eng. Fail. Anal.* **2019**, *97*, 493–505.
23. Luo, S.; Liu, M.; Zheng, X. Characteristics and life expression of fatigue fracture of drilling pipe steels for API G105 and S135 grade. *Eng. Fail. Anal.* **2020**, *116*, 104705.
24. Zheng, X.-L.; Lu, B.; Jiang, H. Determination of probability distribution of fatigue strength and expressions of P–S–N curves. *Eng. Fract. Mech.* **1995**, *50*, 483–491.
25. Wang, R. *Corrosion Fatigue of Metallic Materials [M]*; Xi'an Northwestern Polytechnical University Press: Xi'an, China, 2001.
26. Zheng, X.L.; Wang, R. Overload effects on corrosion fatigue crack initiation life and life prediction of aluminum notched elements under variable amplitude loading. *Eng. Fract. Mech.* **1999**, *57*, 557–572.

27. Bhattacharjee, S.; Dhar, S.; Acharyya, S.K.; Gupta, S.K. Modelling of non-proportional hardening by dislocation based latent effects for SA333 Grade-6 C-Mn Steel. *Mater. Res. Express* **2019**, *6*, 086562.
28. Borodii, M.V. Determination of the Non-Proportional Cyclic Hardening Coefficient Sensitive to the Loading Amplitude. *Strength Mater.* **2021**, *52*, 919–929.
29. Zhang, Q.; Hu, X.; Zhang, Z.; Sun, T.; Wu, J.; Li, Y.; Ren, T. The mean stress and phase angle effect on multiaxial fatigue behavior of a TiAl alloy: Failure analysis and life modeling. *Int. J. Mech. Sci.* **2021**, *193*, 106123.
30. Amjadi, M.; Fatemi, A. Multiaxial Fatigue Behavior of Thermoplastics Including Mean Stress and Notch Effects: Experiments and Modeling. *Int. J. Fatigue* **2020**, *136*, 105571.
31. Zhao, B.; Xie, L.; Wang, L.; Hu, Z.; Zhou, S.; Bai, X. A new multiaxial fatigue life prediction model for aircraft aluminum alloy. *Int. J. Fatigue* **2021**, *143*, 105993.
32. Shu, D.L. *Mechanical Properties of Engineering Materials*; China Machine Press: Beijing, China, 2007.
33. Luo, S.-J.; Wang, R.; Zhao, K. Investigations of fatigue performance of S135 drill pipe steel under uniaxial loading. *Adv. Mater. Res.* **2013**, *716*, 418–422.
34. Carpinteri, A.; Spagnoli, A. Multiaxial high-cycle fatigue criterion for hard metals. *Int. J. Fatigue* **2001**, *23*, 135–145.
35. Findley, W.N. A theory for the effect of mean stress on fatigue of metals under combined torsion and axial load or bending. *J. Eng. Ind.* **1959**, *81*, 301–306.
36. Matake, T. An explanation on fatigue limit under combined stress. *Bull JSME* **1977**, *141*, 257–263.
37. Park, J.; Nelson, D. Evaluation of an energy-based approach and a critical plane approach for predicting constant amplitude multiaxial fatigue life. *Int. J. Fatigue* **2000**, *22*, 23–39.
38. Freitas, M.D.; Li, B.; Santos, J.L. A numerical approach for high-cycle fatigue life prediction with multiaxial loading. In *Multiaxial Fatigue and Deformation: Testing and Prediction*; Kalluri, S., Bonacuse, P., Eds.; ASTM: West Conshohocken, PA, USA, 2000; pp. 139–156.